

## COSMOLOGICAL CONSTRAINTS FROM THE REDSHIFT DEPENDENCE OF THE GALAXY ANGULAR 2-POINT CORRELATION FUNCTION

XIAO-DONG LI,

School of Physics, Korea Institute for Advanced Study, 85 Heogiro, Dongdaemun-gu, Seoul 130-722, Korea

CHENG CHENG,

Kavli Institute for Theoretical Physics China, Institute of Theoretical Physics, Chinese Academy of Sciences, Zhong Guan Cun Street 55#, Beijing, 100190, P.R. China and  
 University of Chinese Academy of Sciences, P.R. China

CHANGBOM PARK,

School of Physics, Korea Institute for Advanced Study, 85 Heogiro, Dongdaemun-gu, Seoul 130-722, Korea

HYUNBAE PARK, CRISTIANO G. SABIU,

Korea Astronomy and Space Science Institute, Daejeon 305-348, Korea

JUHAN KIM<sup>1</sup>,

Center for Advanced Computation, Korea Institute for Advanced Study, 85 Hoegi-ro, Dongdaemun-gu, Seoul 130-722, Korea and  
 School of Physics, Korea Institute for Advanced Study, 85 Heogiro, Dongdaemun-gu, Seoul 130-722, Korea

AND

SUNGWOOK E. HONG

School of Physics, Korea Institute for Advanced Study, 85 Heogiro, Dongdaemun-gu, Seoul 130-722, Korea

*Draft version September 9, 2016*

### ABSTRACT

We use the shape of galaxy 2-point correlation function to measure the redshift dependence cosmology volume effect. ...

*Keywords:* large-scale structure of Universe — dark energy — cosmological parameters

### 1. INTRODUCTION

Dark energy ... Large scale structure...

2pCF is a good statistic... blahblah In 2d xi(s,μ)  
 ... In \*\*\* we used the redshift dependence of 2pCF to probe the volume and AP effect... The method is applied to BOSS data in \*\*\* and obtain tight constraint...

In \*\*\* we further propose to use the shape of xi(s) to probe the volume effect... Stretch or compression shifts the clustering properties in some particular scale to larger or smaller scales... The shape of measured xi(s) is thus stretched or compressed.

The outline of this paper is as follows.

This paper is organized as follows... The outline of this paper proceeds as follows. In §2 we briefly review the nature and consequences of the AP effect and volume changes when performing coordinate transforms in a cosmological context. In §3 we describe the N-body simulations and mock galaxy catalogues that are used to test our methodology. In §4, we describe our new analysis method for quantifying the redshift dependence of volume effect. We conclude in §5.

### 2. VOLUME EFFECT IN A NUTSHELL

In this section we briefly introduce the scaling effect caused by wrongly assumed cosmological parameters. A more detailed description has been provided in Li et al. (2014, 2015, 2016).

Suppose that we are probing the size of some objects

in the Universe. We measure its redshift span  $\Delta z$  and angular size  $\Delta\theta$ , then compute its sizes in the radial and transverse directions using the following formulas

$$\Delta r_{\parallel} = \frac{c}{H(z)} \Delta z, \quad \Delta r_{\perp} = (1+z) D_A(z) \Delta\theta, \quad (1)$$

where  $H$  is the Hubble parameter and  $D_A$  is the angular diameter distance. In the particular case of a flat universe composed by a cold dark matter component and a constant EoS dark energy component, they take the forms of

$$H(z) = H_0 \sqrt{\Omega_m a^{-3} + (1 - \Omega_m) a^{-3(1+w)}}, \\ D_A(z) = \frac{1}{1+z} r(z) = \frac{1}{1+z} \int_0^z \frac{dz'}{H(z')}, \quad (2)$$

where  $a = 1/(1+z)$  is the cosmic scale factor,  $H_0$  is the present value of Hubble parameter and  $r(z)$  is the comoving distance.

In case wrong values of  $\Omega_m$  and  $w$  are adopted, the inferred  $\Delta r_{\parallel}$  and  $\Delta r_{\perp}$  are wrong, resulting in wrong estimation in the object's shape (AP effect) and size (volume effect). These effects and their cosmological consequences have been investigated in Li et al. (2014, 2015, 2016).

In this paper we focus on the mis-estimation of the angular size  $\Delta r_{\perp}$ . The ratio of mis-estimation is

$$\alpha_{\perp} \equiv \frac{\Delta r_{\perp,\text{wrong}}}{\Delta r_{\perp,\text{true}}} = \frac{D_{A,\text{wrong}}}{D_{A,\text{true}}}, \quad (3)$$

<sup>1</sup> Corresponding Author: kjhan@kias.re.kr

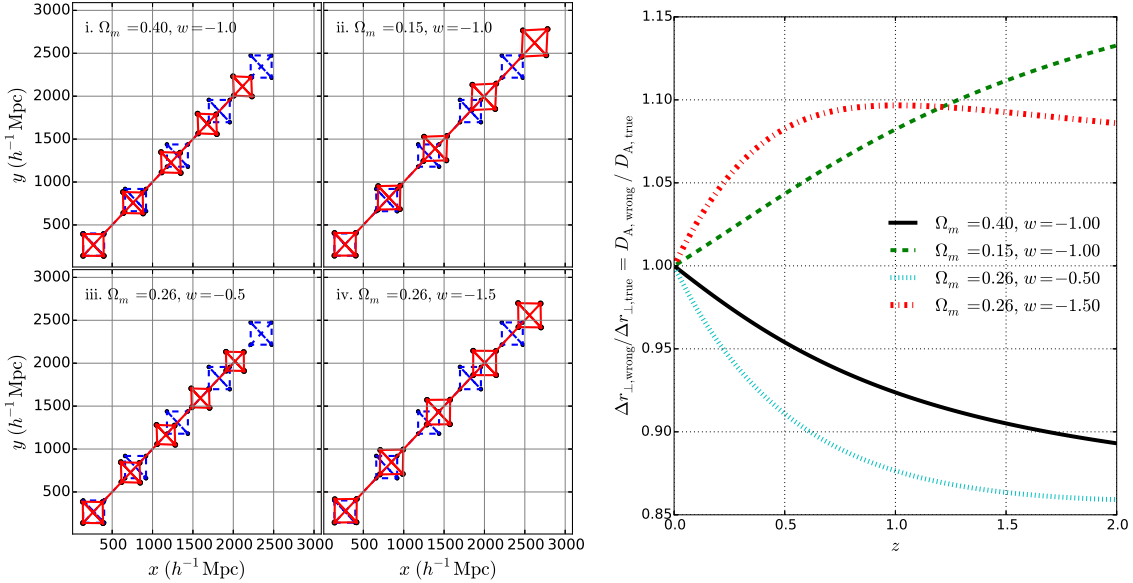


**Figure 1.** The scaling in four wrongly assumed cosmologies ..., assuming a true cosmology of  $\Omega_m = 0.26$ ,  $w = -1$ . Left panel shows a series objects distributes as five perfect squares, measured by an observer located at the origin. Their true positions and shapes are plotted in blue dashed lines. The observer measures the redshifts of these objects, adopts the wrong cosmologies to compute the distance, and obtains wrong results (red solid lines). Right panel shows the mis-estimation of angular diameter distance when the wrong cosmologies are adopted.

where “true” and “wrong” denote the values of  $D_A$  in the true cosmology and wrongly assumed cosmologies, respectively.

An illustration is provided in the left panels of Figure 1. Suppose that the true cosmology is a flat  $\Lambda$ CDM with present matter ratio  $\Omega_m = 0.26$  and standard dark energy EoS  $w = -1$ . If we were to distribute a series of perfect squares at various distances ranging from 500 Mpc/h to 3000 Mpc/h, and an observer located at the origin were to measure their redshifts and infer the sizes of the squares using the distance-redshift relations of four incorrect cosmologies

- (i).  $\Omega_m = 0.40$ ,  $w = -1.0$ ,
- (ii).  $\Omega_m = 0.15$ ,  $w = -1.0$ ,
- (iii).  $\Omega_m = 0.26$ ,  $w = -0.5$ ,
- (iv).  $\Omega_m = 0.26$ ,  $w = -1.5$ ,

as a result, the shapes of the squares appear distorted (AP effect), and their sizes are wrongly estimated (volume effect). Cosmological models (i,iii) yield to compressed size (in both angular and LOS direction), and the degree of compression increases with increasing distance;

The mis-estimation of angular size,  $\Delta r_{\perp,\text{wrong}} / \Delta r_{\perp,\text{true}}$ , are displayed in the right panel of Figure 1. All cosmologies,  $\Delta r_{\perp,\text{wrong}} / \Delta r_{\perp,\text{true}}$  evolves a lot in the redshift range  $0 < z < 2$ . As an example, when adopting the quintessence cosmology  $\Omega_m = 0.26$ ,  $w = -0.5$ , the angular size is underestimated by 8.9%, 12.3%, 13.6%, 14.1% at  $z = 0.5, 1, 1.5, 2$ .

In sum, as a consequence of incorrectly adopted cosmologies, the size of the objects is mis-estimated and the magnitude of mis-estimation depends on the redshift. In this paper we use the galaxy angular 2pCF to probe the mis-estimation of angular size  $\Delta r_{\perp,\text{wrong}} / \Delta r_{\perp,\text{true}}$ .

### 3. THE SIMULATION DATA

We test the method using the mock galaxy samples produced by the Horizon Run 4 (HR4) N-body simulation (Kim et al. 2015; Hong et al. 2016).

HR4 was made within a cube of volume  $(3.15 h^{-1} \text{Gpc})^3$  using  $6300^3$  particles with mass  $m_p \simeq 9 \times 10^9 h^{-1} \text{M}_\odot$ . The simulation adopted the second order Lagrangian perturbation theory (2LPT) initial conditions at  $z_i = 100$  and a WMAP5 cosmology  $(\Omega_b, \Omega_m, \Omega_\Lambda, h, \sigma_8, n_s) = (0.044, 0.26, 0.74, 0.72, 0.79, 0.96)$  (Komatsu et al. 2011).

Mock galaxies are produced from the simulation based on a modified one-to-one correspondence scheme (Hong et al. 2016). The most bound member particles (MBPs) of simulated halos are adopted as tracers of galaxies. The merger timescale is computed to get the lifetime of merged halos. Merger trees of halos are constructed by tracking their MBPs from  $z = 12$  to 0; when a merger event occurs, the merger timescale is computed using the formula of Jiang et al. (2008) to determine when the satellite galaxy is completely disrupted.

The resulting mock galaxies was found to reproduce the 2pCF of SDSS DR7 volume-limited galaxy sample (Zehavi et al. 2011) very well (Hong et al. 2016). The mock galaxies shows a similar finger of god (FOG) feature (Jackson 1972) as the observation. The projected 2pCF of the mock and observational samples agree within  $1\sigma$  CL on scales greater than  $1 h^{-1} \text{Mpc}$ .

In this analysis we use snapshot data of HR4 galaxies at  $z = 0, 0.5, 1, 1.5, 2$ . Setting a minimal halo mass of  $3 \times 10^{11} h^{-1} \text{M}_\odot$ , we select 457, 406, 352, 206 and 228 million mock galaxies at the five redshifts, corresponding to a number density of 1.46, 1.30, 1.13, 0.98 and 0.73 in unit of  $10^{-2} h^3 \text{Mpc}^{-3}$ , respectively. By applying a uniform mass cut, at higher redshift we are selecting less galaxies with larger galaxy bias.

As an illustration, Figure 2 displays the 2D distribution of a subsample of mock galaxies in five redshifts, with  $x, y$  coordinates computed using the “correct” val-

ues of cosmological parameters  $\Omega_m = 0.26$ ,  $w = -1$  (left panels) and a wrong set of cosmological parameters  $\Omega_m = 0.05$ ,  $w = -1.5$  (right panels), respectively.

When the correct cosmology is adopted the cosmic scale is correctly estimated in five redshifts. The only factor leads to evolution of galaxy distribution with redshift is the gravitational growth of structure. With the decreasing the redshift, we clearly see how the clusters and filaments form and grow. On the other hand, when the wrong cosmology is adopted, there is an artificial scaling of scales in the constructed map. The separations among galaxies are overestimated by 25.6%, 47.3%, 62.2%, 71.7% at redshifts of 0.5, 1.0, 1.5, 2.5, leading to a clear evolution of the sizes of structures with redshift.

The growth of structure leads to growth of clustering strength of structures on all scales, while the volume effect maintain the clustering pattern and uniformly rescale all the structures. Their imprints on the large scale structure is different and should be distinguishable in the statistical analysis. In the following, we show that they affect the angular correlation function measurements in different ways, and can be easily separated.

The growth of structure also make the size of structures evolves with redshift. In the next subsection we will discuss how to distinguish these two effects in the galaxy angular 2pCF.

#### 4. METHODOLOGY

We use the angular 2pCF as a statistical tool to probe the volume effect. The galaxy 2pCF as a function of galaxy separation in the angular direction,  $\omega(r_\perp)$ , is computed for snapshot data of mock galaxies at five redshifts. We adopt the Landy-Szalay estimator (Landy & Szalay 1993),

$$\omega(r_\perp) = \frac{DD - 2DR + RR}{RR}, \quad (4)$$

where  $DD$  is the number of galaxy-galaxy pairs,  $DR$  the number of galaxy-random pairs, and  $RR$  is the number of random-random pairs, all separated by a distance defined by  $r_\perp \pm \Delta_{r_\perp}$  where we choose  $\Delta_{r_\perp} = 1h^{-1}\text{Mpc}$ . The random catalogue consists of unclustered points uniformly distributed in a same size box. In an effort to reduce the statistical variance of the estimator, we use 50 times as many random points as we have galaxies.

Considering the large number of galaxies and random points the 2pCF is computed part by part in subsamples with size of  $1575 h^{-1}\text{Mpc} \times 1575 h^{-1}\text{Mpc} \times 105 h^{-1}\text{Mpc}$ . The Z direction with thickness  $105 h^{-1}\text{Mpc}$  is treated as the radial direction and the X, Y direction with width  $1575 h^{-1}\text{Mpc}$  are treated as the angular plane. In our simulation box we can have 120 such subsamples. The average of the measurements in all subsamples is adopted as the 2pCF of the whole sample, while the covariances of them are adopted as the covariance matrix after multiplying a factor of  $1/\sqrt{119}$ .

#### 4.1. Galaxy angular 2pCF: amplitude and shape at different redshifts

The upper-left panel of Figure 3 displays the angular 2pCF measured from HR4 mock galaxies. We multiply  $\omega$  by the separation  $r_\perp$  to have similar amount of statistical uncertainty on all scales.

At different redshifts, we see large evolution in the amplitude of  $\omega(r_\perp)$ . The amplitude of 2pCF is proportional

to the clustering strength which is affected by the gravitational growth of structures and the bias of the galaxies. The amplitude is highest at  $z = 0$  where the large scale structures experienced most gravitational growth, and also gets higher at  $z > 1$  with increasing redshift as a reason of more biased galaxies at higher redshift.

Different from the large variation of amplitude among the different redshifts, the shape of  $r_\perp\omega$  maintains similar at all redshifts; it always peaks at  $r \sim 9h^{-1}\text{Mpc}$  and monotonically drops at larger or smaller scales. The only exception is the small enhancement at  $r \lesssim 2h^{-1}\text{Mpc}$ , which is caused by the non-linear growth of structures on small scales and is much more significant at lower redshift.

In order to directly compare the shape of 2pCF at different redshifts, in the middle panel of Figure 3 we show the  $r_\perp\omega$  normalized by the overall amplitude within  $5h^{-1}\text{Mpc} < r < 50h^{-1}\text{Mpc}$  (here after  $\hat{r}_\perp\omega$ ). The nice overlapping of the five redshift results justify the small evolution of shape with redshift. In the right panel, we further show the residual evolution of  $\hat{r}_\perp\omega$  at high redshifts with respect to  $z = 0$ . There is only 1-4% relative enhancement at  $r < 10h^{-1}\text{Mpc}$ , and < 1.5% relative suppression at  $r > 25h^{-1}\text{Mpc}$ . The trend is monotonic with redshift.

As shown by Figure 2, the gravitational growth of structure enhance the clustering strength of structures on all scales; here it manifests itself as an enhanced amplitude of 2pCF at low redshift. The shape of 2pCF, which represents the *relative strength of clustering among different scales*, maintain similar with redshift except the non-linear scales of  $r_\perp < 5h^{-1}\text{Mpc}$ .

#### 4.2. Galaxy angular 2pCF: in wrong cosmologies

When a wrong set of cosmological parameters is adopted, the galaxy distribution is artificially scaled. This scaling is expected to change the shape of the 2pCF, following the relationship,

$$\hat{\omega}_{\text{wrong}}(r) = \hat{\omega}_{\text{true}}(\alpha_\perp r), \quad (5)$$

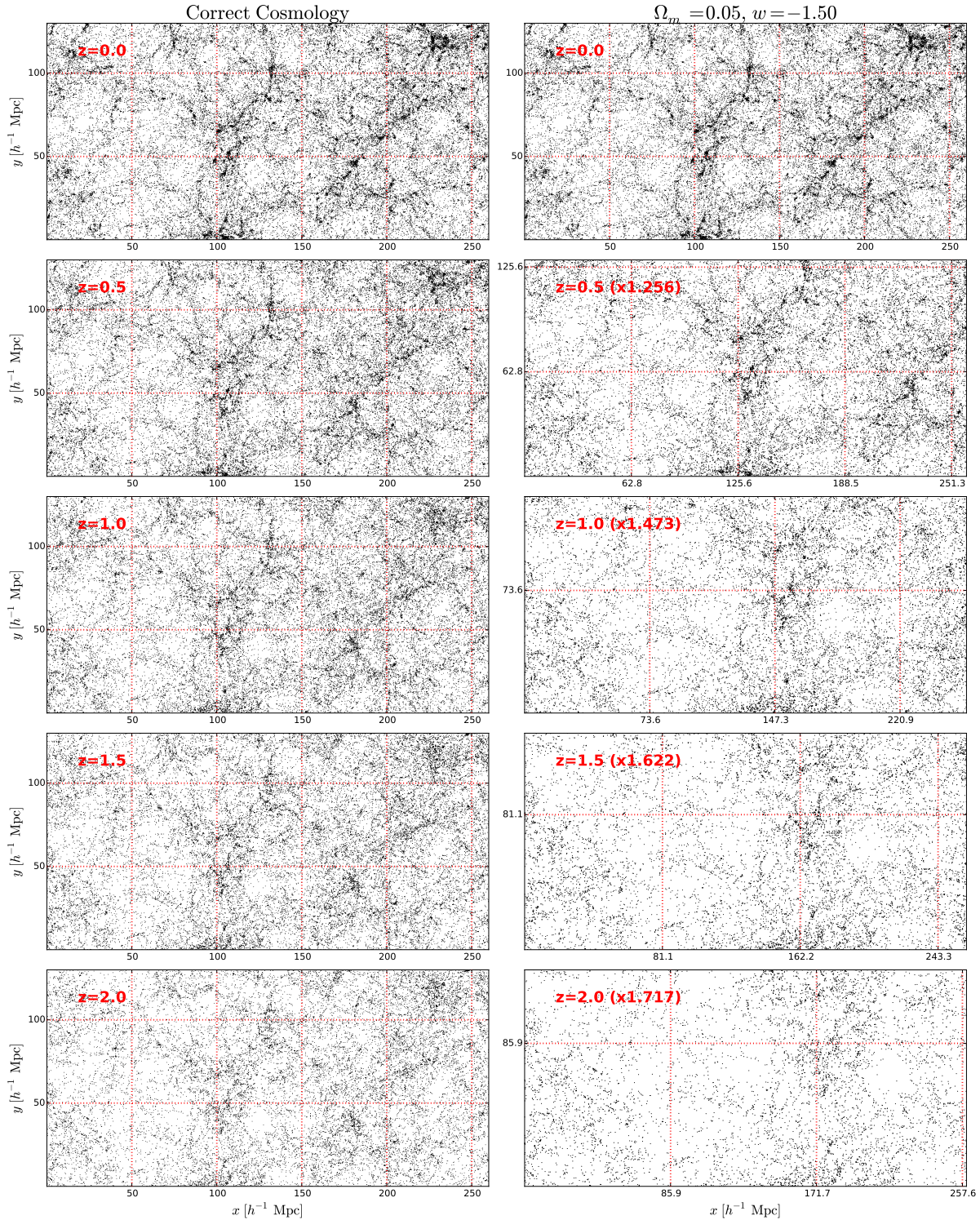
a simple consequence of the fact that clustering patterns at distance  $r$  now appears on a the scale  $\alpha_\perp r$ . The redshift evolution of  $\alpha_\perp$  leads to redshift evolution of shape.

Lower panels of Figure 3 shows the  $r_\perp\omega$  in five snapshots, in case that the cosmology  $\Omega_m = 0.05$ ,  $w = -1.5$  is adopted to construct the galaxy distribution (the right panels of Figure 2). The middle panel displays the clear redshift evolution of shape of  $r_\perp\omega$ . E.g., from  $z = 0$  to  $z = 2$ , the peak location is shifted from  $r = 9h^{-1}\text{Mpc}$  to  $r \sim 15h^{-1}\text{Mpc}$  at  $z = 2$  since the angular separation is upscaled by 71.7%.

The right panel shows that, at higher redshift, there is a 20-40% change in the value of  $\hat{r}_\perp\omega$ .

The amplitude of  $r_\perp\omega$  is amplified due to the stretch of scale. As shown in the left panel, the amplitude monotonically increases as a function of redshift. But this phenomenon can also appear in case of gravitational growth of structure or increasing of bias, so we will not make use of it to do cosmological constraint. We utilize the redshift evolution of the 2pCF shape as a signal suggesting that the assumed cosmological parameters are wrong.

In Figure 5 we further plot the redshift evolution of 2pCF in the four wrong cosmologies of Figure 1. In all cases, the scaling leads to evident redshift evolution of the shape of  $r_\perp\omega$ . When the cosmologies  $\Omega_m = 0.4$ ,  $w = -1$  and  $\Omega_m = 0.26$ ,  $w = -0.5$  are adopted, the com-

**Figure 2.** blah

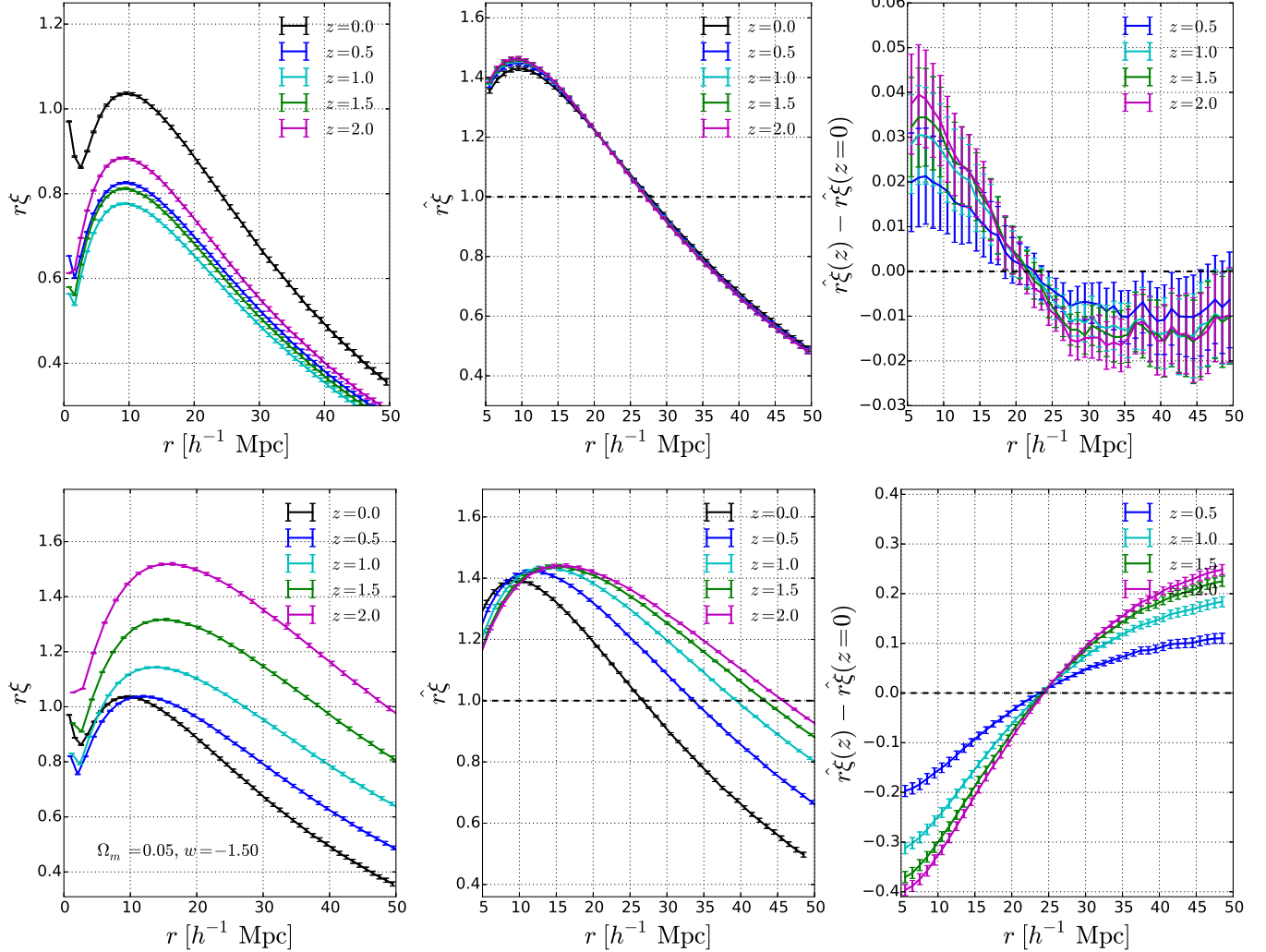


Figure 3. 2pCF at different redshifts.

pression of structure makes the clustering patterns appears on smaller scales. This leads to “steeper” slope of  $r_{\perp}\omega$ , and the higher the redshift, the steeper the slope. To the opposite, when adopting the cosmologies  $\Omega_m = 0.15, w = -1$  and  $\Omega_m = 0.26, w = -1.5$ , the stretch of size makes the slope shallower at higher redshifts.

#### 4.3. Systematic effects

The same as Li et al. (2014, 2015, 2016) we need to correct for the redshift evolution of  $r_{\perp}\omega$  caused by effects other than the cosmological effect.

Figure 3 already shows that, the growth of structure, especially in low redshift and on non-linear scales, changes the shape of  $r_{\perp}\omega$  and caused relative enhancement on  $r \lesssim 2h^{-1}\text{Mpc}$ . So we limit the region of scale to  $r > 5h^{-1}\text{Mpc}$  to minimize its effect.

Galaxies are biased tracers of dark matter field, and more massive galaxies tend to reside in regions with higher density contrast. So in large scale structure surveys the bias of the galaxy sample is an important factor which has large effect on the clustering properties of the sample. The upper panels of Figure 4 displays five set of galaxy samples in a  $3175 \times 3175 \times 105$  ( $h^{-1}\text{Mpc}$ )<sup>3</sup> volume, taken from the  $z = 0$  snapshots data. Different lower mass limits of  $3 \times 10^{11} M_{\odot}$ ,  $3 \times 10^{11} M_{\odot}$ ,  $3 \times 10^{11} M_{\odot}$  and  $3 \times 10^{11} M_{\odot}$  are imposed to create subsamples with different galaxy bias, and the measured angular 2pCF are displayed. The different mass cuts result in large variation in the amplitude of the 2pCF (left panel), while the shape of the 2pCF remains less affected (middle panel). Compared with the sample with mass cut  $M > 3 \times 10^{11} M_{\odot}$ , samples with mass limit  $3 \times 10^{11} M_{\odot}$ ,  $3 \times 10^{11} M_{\odot}$  and  $3 \times 10^{11} M_{\odot}$  have the amplitude of 2pCFs enhanced by 10%, 50% and 100%, while the change in  $r_{\perp}\omega$  is only 0.5%, 2% and 4%. Considering the very large change in the mass cut, the change in the shape of 2pCF is not significant.

The galaxy peculiar velocity contribute to the observed galaxy redshift and distorted the galaxy radial position in redshift space, known as the redshift space distortion (RSD). It is the major source of systematics for our analysis of Li et al. (2014, 2015, 2016), where the 3D galaxy distribution is utilized to derive cosmological constraint. In this analysis its effect becomes much milder since the angular positions of the galaxies is not affected by RSD at all. But it still affects our analysis in the procedure of preparing the subsamples of galaxies for 2pCF analysis. The galaxies observed in a survey are split into shells or subsamples, with different redshift ranges, to get the 2pCF at different redshifts. RSD distorts the galaxy redshift and as a result some galaxies close the boundaries of shells will be distributed to wrong redshift shells.

The lower panel of Figure 4 displays the RSD effect on 2pCF. To mimick the effect of RSD we shift the  $Z$  coordinates of galaxies according to the relation

$$\Delta z = (1+z) \frac{v_Z}{c}, \quad (6)$$

where  $v_Z$  is the galaxy peculiar velocity in  $Z$  direction. Then we split the whole box into 30 slices with thickness  $105h^{-1}\text{Mpc}$ , and measure the angular 2pCF. The left panel shows that the amplitude of measured 2pCF is enhanced by  $\sim 10\%$  in case of considering the RSD effect on splitting samples. The middle panel shows that the shape of 2pCF is also altered – the slop is suppressed. If looking

at the redshift evolution, the curves  $r_{\perp}\hat{\omega} - r_{\perp}\hat{\omega}(z=0)$  displayed in the right panel, they changed a lot compared with the case of no RSD effect (the right panel of Figure 3), but do not become much larger.

Similar to RSD, the redshift errors in survey can affect the subsamples of galaxies by buring the boundaries of shells. This effect should be properly quantified, especially in case of a photometric survey where the redshift uncertainty can be  $\Delta z \approx 0.02$ .

In Li et al. (2014, 2015, 2016), the systematic effects contributing to the redshift evolution of galaxy clusterings are modeled in mock surveys and subtracted. Similar treatment could be conducted here. One shall construct mock surveys with the above effects included for the correction of systematics.

#### 4.4. Likelihood Analysis

We build up a likelihood function to describe how significant is the redshift evolution of the 2pCF shape, so that to determine whether the adopted cosmological parameters are correct. The redshift evolution is characterized by the difference between the  $r_{\perp}\hat{\omega}$  measured in the lowest redshift and higher ones; the cosmology having least redshift evolution of  $r_{\perp}\hat{\omega}$  is considered to be the most plausible one and has smallest  $\chi^2$ . So we have

$$\chi^2 \equiv \sum_{i=2}^{n_z} \sum_{j_1=1}^{n_r} \sum_{j_2=1}^{n_r} \mathbf{p}(z_i, r_{j_1}) (\mathbf{Cov}_i^{-1})_{j_1, j_2} \mathbf{p}(z_i, r_{j_2}), \quad (7)$$

where  $n_z$  is the number of redshifts,  $n_r$  is number of bins in  $r_{\perp}\hat{\omega}(r)$ ; in this analysis we have five redshift bins, and 35  $r$  bins with bin width  $1h^{-1}\text{Mpc}$  in the range  $5h^{-1}\text{Mpc} < r < 40h^{-1}\text{Mpc}$ .  $\mathbf{p}(z_i, r_j)$  is the redshift evolution of clustering,  $r_{\perp}\hat{\omega}$ , with systematic effects subtracted

$$\mathbf{p}(z_i, r_j) \equiv \delta r_{\perp}\hat{\omega}(z_i, z_1, r_j) - \delta r_{\perp}\hat{\omega}_{\text{sys}}(z_i, z_1, r_j) \quad (8)$$

$\mathbf{Cov}_i$  is the covariance matrix.

It is difficult to conduct the 2pCF of the whole snapshot box with hundreds of millions of galaxies. We split the box into 120 subsamples with  $X, Y, Z$  sizes of  $1575h^{-1}\text{Mpc}$ ,  $1575h^{-1}\text{Mpc}$ ,  $105h^{-1}\text{Mpc}$  and measure the angular 2pCF in the  $X-Y$  plan in these subsamples. The average of the 2pCFs are taken as the 2pCF of the whole box. The covariance matrix is also estimated from these 2pCFs.

In real observations we observe *different* objects at different redshift shells. To mimick this when calculating the redshift evolution of 2pCF we use subsamples at different positions at different redshifts. E.g., if for the  $z = 0$  snapshot we use the  $r_{\perp}\hat{\omega}$  measured in the subsample  $0h^{-1}\text{Mpc} < Z < 105h^{-1}\text{Mpc}$ , at higher redshifts we adopt the  $r_{\perp}\hat{\omega}$  measured in a subsample  $105h^{-1}\text{Mpc} < Z < 210h^{-1}\text{Mpc}$ , and take the difference between them to get  $\delta r_{\perp}\hat{\omega}$ . So we are always comparing 2pCF measured from different samples of galaxies. If simply comparing the 2pCF of a same sample of galaxies at different redshifts, one would significantly underestimate the statistical uncertainty of  $\delta r_{\perp}\hat{\omega}$  by ignoring the cosmic variance <sup>2</sup>.

<sup>2</sup> The error bars displayed in all figures are estimated from the 120 subsamples and for the error bar of redshift evolution of 2pCF we always take the cosmic variance into consideration.

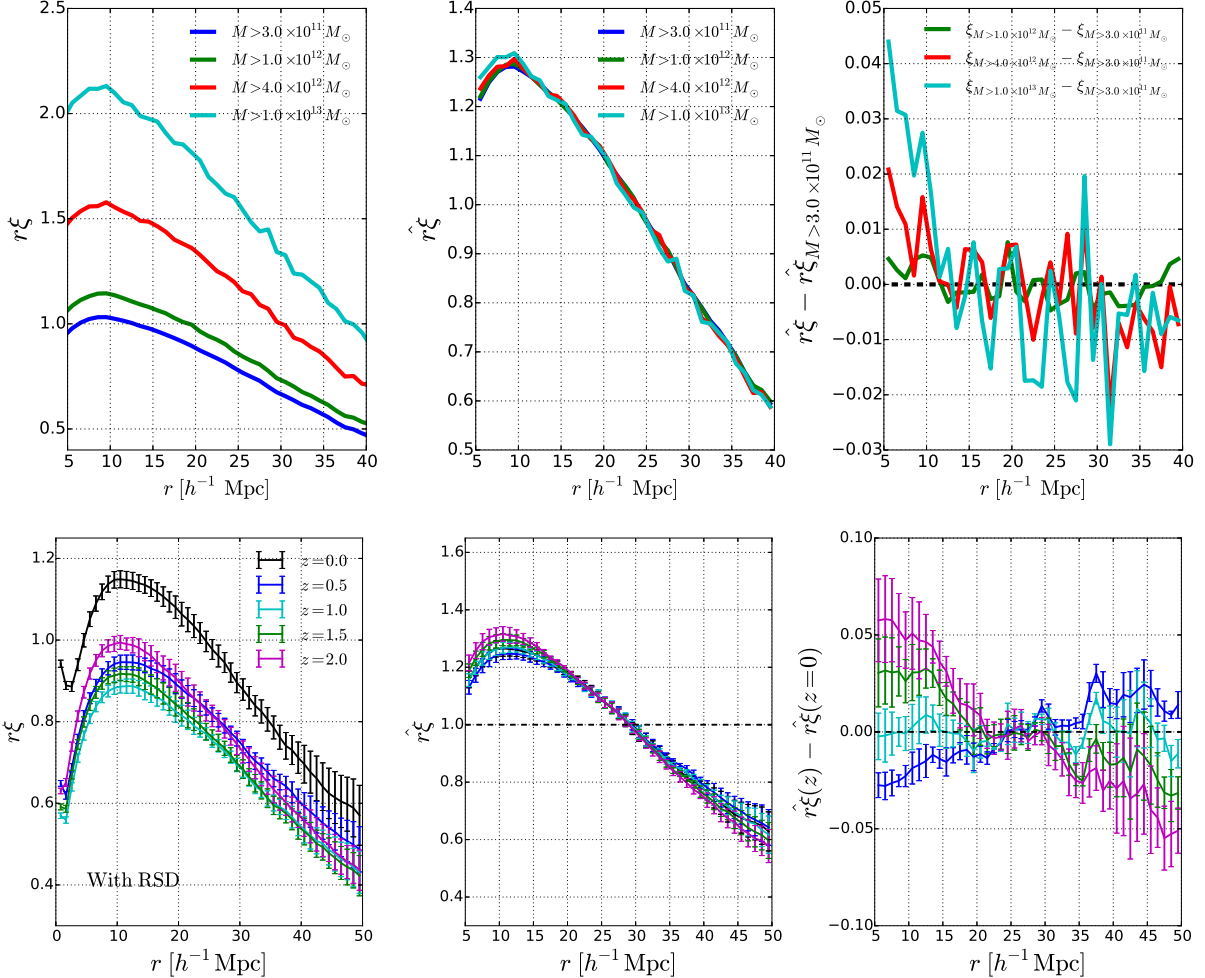


**Figure 4.** Systematic effects.

Figure 5 displayed the 2pCF measured in the four cosmologies displayed in Figure 1. For the cosmologies  $\Omega_m = 0.4, w = -1$  and  $\Omega_m = 0.26, w = -0.5$ , the compression of structure rescale large scale clustering patterns into small scales; the compression becomes more significant at higher redshift. In these cosmologies we get 2pCFs with steeper slope and, the higher redshift, the steeper. For  $\Omega_m = 0.15, w = -1$  and  $\Omega_m = 0.26, w = -1.5$ , the stretch of structure leads to shallower slope of  $r\hat{\omega}$  and, the higher the redshift, the shallower. In all cosmologies we find significant detection of redshift evolution of  $r\hat{\omega}$  (in the lowest panels,  $\delta r\hat{\omega} \neq 0$ ). We computed the  $\chi^2$  values according to Equation 7 and found these sets of cosmological parameters are strongly disfavored at  $\gtrsim 30\sigma$  CL.

## 5. COSMOLOGICAL CONSTRAINT

We constrain  $\Omega_m$  and  $w$  through Bayesian analysis ((Christensen et al. 2001); also see (Lewis & Bridle 2002; Li et al. 2016) for details). We assume the likelihood takes the form

$$\mathcal{L} \propto \exp \left[ -\frac{\chi^2}{2} \right] \quad (9)$$

and scan the parameter space in  $\Omega_m - w$  plane to obtain the 68.3% and 97.4% CL regions. The result is displayed in Figure ??.

We get tight constraint on the two parameters. The  $2\sigma$  contour lies within the region  $0.23 < \Omega_m < 0.285$ ,  $-1.1 < w < -0.9$ . The thin shape of contour means, when combining with the another observational data with different direction of degeneracy (e.g. CMB), very tight combined constraint can be obtained. In case of fixing one parameter at its best-fit value and infer the statistical uncertainty of the other one, one will obtain  $1\sigma$  uncertainty of  $\delta\Omega_m \approx 0.002$ ,  $\delta w \approx 0.01$ .

## 6. CONCLUDING REMARKS

\* Can be combined with our redshift dependence of AP to full explore the geometric effects in LSS

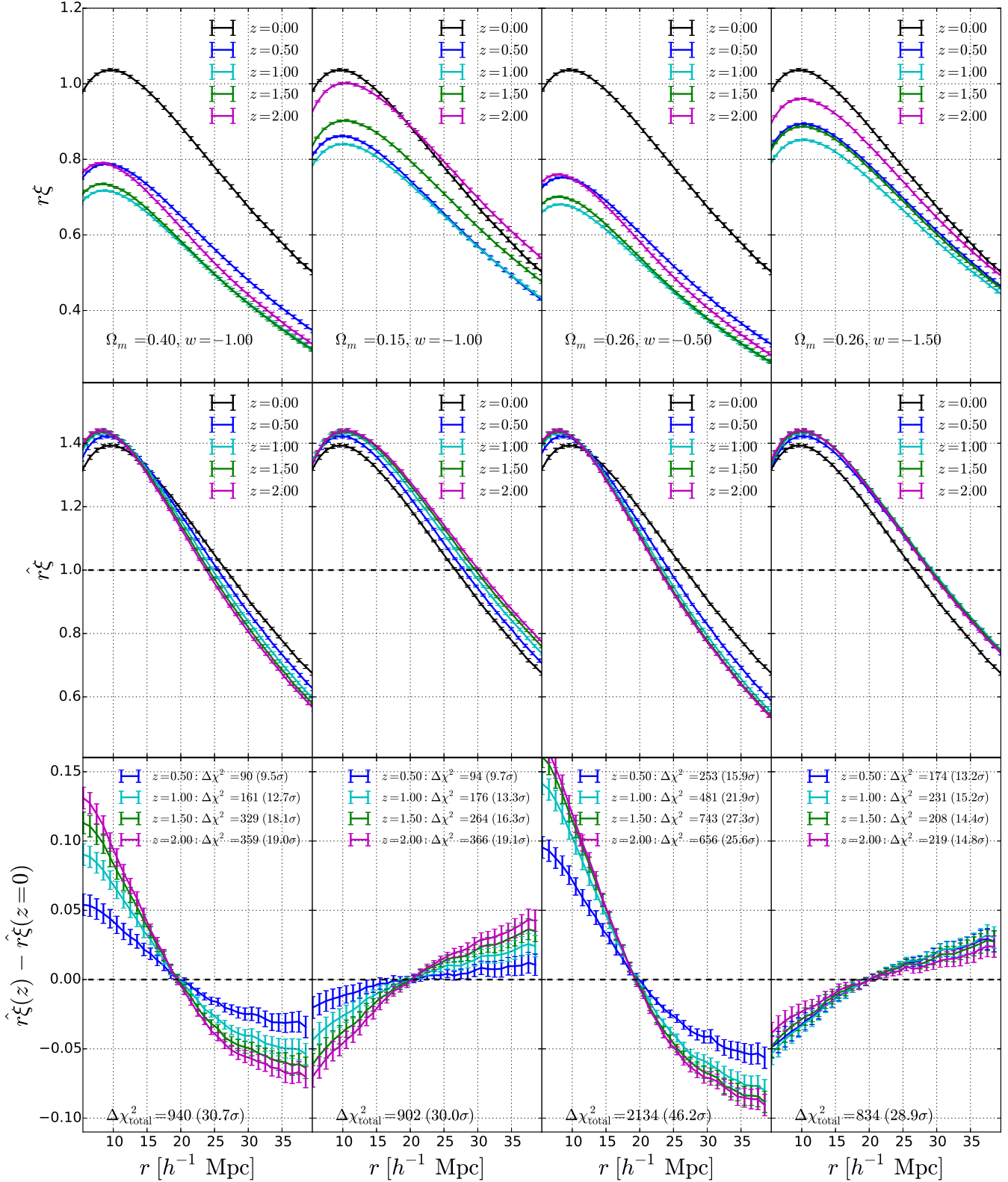
\* \*\*\* utilizes angular 2pCF as a function of redshift. Our method is complementary to it: 1) smaller scales; 2) more bins; 3) could be less affected by RSD; ... In case of good modelling of RSD one can rely on their; in case not possible, especially on small scales, one can use ours

\* Complementary to all other LSS probes

\* Promising future

## ACKNOWLEDGMENTS

We thank the Korea Institute for Advanced Study for providing computing resources (KIAS Center for Advanced Computation Linux Cluster System). We would like to thank Yi Zheng for useful discussions. This work was partially supported by the Supercomputing Center/Korea Institute of Science and Technology Informa-



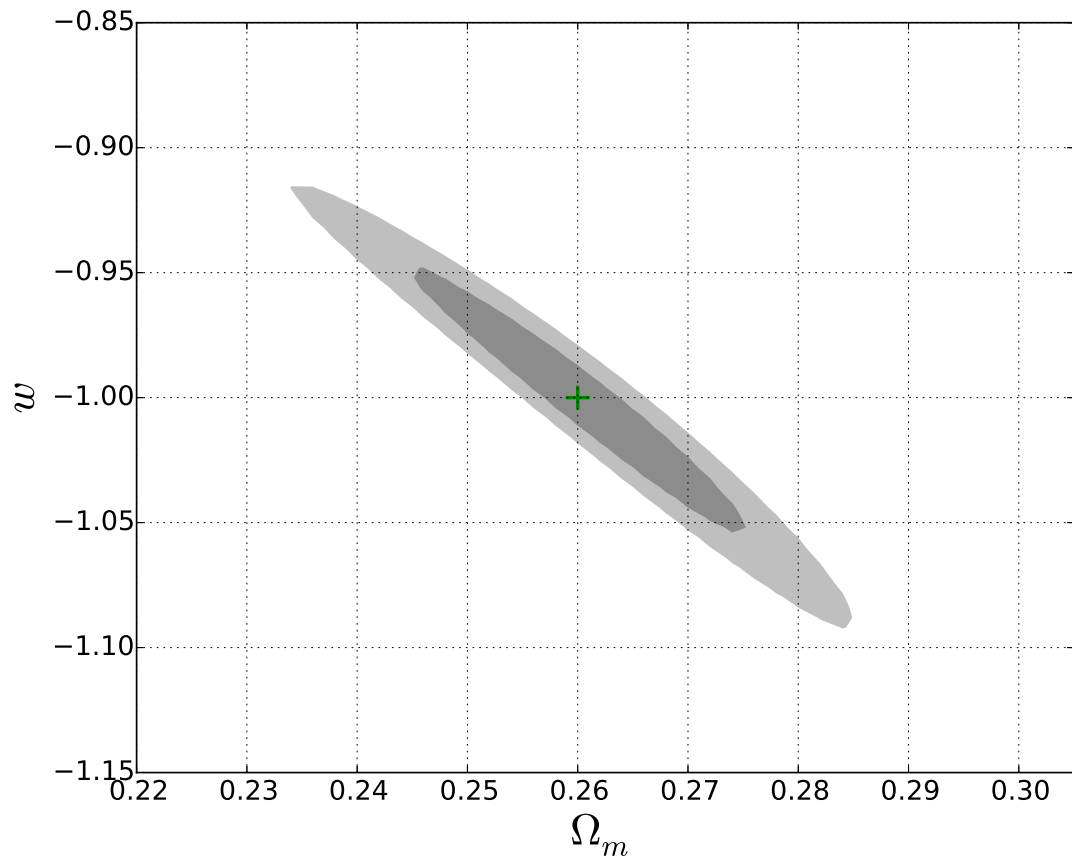


**Figure 6.** Likelihood contours (68.3%, 95.4%) in the  $\Omega_m - w$  plane from our method.

tion with supercomputing resources including technical

support (KSC-2013-G2-003).

## APPENDIX

### REFERENCES

- Ade, P.A.R., Aghanim, N., & Arnaud, M., et al. arXiv:1502.01589
- Alam, S., Ata, M., & Bailey, S., et al. 2016, submitted to MNRAS (arXiv:1607.03155)
- Alam S., Albareti, F.D., & Allende Prieto, C., et al., 2015, ApJS, 219, 12
- Alcock, C., & Paczynski, B. 1979, Nature, 281, 358
- Anderson, L., Aubourg, É., & Bailey, S. et al. 2014, MNRAS, 441, 24
- Ballinger, W.E., Peacock, J.A., & Heavens, A.F. 1996, MNRAS, 282, 877
- Betoule, M., Kessler, R., & Guy, J., et al. 2014, A&A, 568, 32
- Beutler, F., Blake, C., & Colless, M., et al. 2011, MNRAS, 416, 3017
- Beutler, F., Saito, S., & Seo, H.-J., et al. 2013, MNRAS, 443, 1065
- Beutler, F., Seo, H.-J., & Saito, S., et al. 2016, arXiv:1607.03150
- Blake, C., Glazebrook, K., & Davis, T. M., 2011, MNRAS, 418, 1725
- Blake, C., James, J.B., & Poole, G.B. 2013, MNRAS, 437, 2488
- Bolton, A.S., Schlegel, & D.J., Aubourg E., et al. 2012, AJ, 144, 144
- Boylan-Kolchin, M., Ma, C.-P., & Quataert, E. 2008, MNRAS, 383, 93
- Christensen, N., Meyer, R., Knox, L., & Luey, B. 2001, Class. Quant. Grav., 18, 2677
- Chuang, C.-H., & Wang, Y. 2012, MNRAS, 426, 226
- Dawson, K.S., Kneib, J.P., & Percival, W.J., et al. 2015, accepted AJ
- Dawson, K.S., Schlegel, D.J., & Ahn, C.P., et al. 2012, AJ, 145, 10
- Efstathiou, G. 2014, MNRAS, 440, 1138
- Eisenstein, D.J., Weinberg, D.H., & Agolet, E., et al. 2011, AJ, 142, 72
- Feldman, H.A., Kaiser, N., & Peacock, J.A. 1994, ApJ, 426, 23
- Fukugita, M., Ichikawa, T., & Gunn, J.E., et al. 1996, AJ, 111, 1748
- Gunn, J.E., Carr, M., & Rockosi, C. et al. 1998, AJ, 116, 3040
- Gunn, J.E., Siegmund, W.A., & Mannery, E.J., et al. 2006, AJ, 131, 2332
- Guzzo, L., Pierleoni, M., & Meneux, B., et al. 2008, Nature, 451, 541
- Hartlap J., Simon P. & Schneider P. [astro-ph/0608064].
- Hong, S.E., Park, C., & Kim, J. 2016, ApJ, 823, 103
- Jackson, J., 1972, MNRAS, 156, 1
- Jennings, E., Baugh, C.M., & Pascoli, S. 2011, MNRAS, 420, 1079
- Jiang, C.Y., Jing, Y. P., & Faltenbacher, A., et al. 2008, ApJ, 675, 1095
- Kaiser, N. 1987, MNRAS, 227, 1
- Kim, J., & Park, C. 2006, ApJ, 639, 600
- Kim, J., Park, C., Gott, J.R., III, & Dubinski, J. 2009, ApJ, 701, 1547
- Kim, J., Park, C., L'Huillier, B., & Hong, S. E. 2015, JKAS, 48, 213
- Kim, J., Park, C., Rossi, G., Lee, S.M., & Gott, J.R. 2011, JKAS, 44, 217
- Kitaura, F.S., Rodríguez-Torres, S., Chuang, C.-H., et al. arXiv:1509.06400
- Komatsu, E., Smith, K. M., & Dunkley, J., et al. 2011, ApJS, 192, 18
- Lacey, C., & Cole, S. 1993, MNRAS, 262, 627
- Landy, S.D., & Szalay, A.S. 1993, ApJ, 412, 64
- Laureijs, R., Amiaux, J., & Arduini, S., et al. 2011, arXiv:1110.3193
- Lavaux, G., & Wandelt, B.D. 2012, ApJ, 754, 109
- Lewis, A., & Bridle, S. 2002, Phys. Rev. D, 66, 103511
- L'Huillier, B., Park, C., & Kim, J. 2014, New Astronomy, 30, 79
- Li, M., Li, X.-D., Wang, S., & Wang, Y. 2011, Commun. Theor. Phys., 56, 525
- Li, X.-D., Park, C., Forero-Romero, J., & Kim, J. 2014, ApJ, 796, 137
- Li, X.-D., Park, C., Sabiu, C.G., & Kim, J. 2015, MNRAS, 450, 807
- Li, X.-D., Park, C., Sabiu, C.G., & Kim, J. 2016, submitted to ApJ
- Linder, E.V., Minji, O., Okumura, T., Sabiu, C.G., & Song, Y.-S. 2014, Phys. Rev. D, 89, 063525
- López-Corredoira, M. 2014, ApJ, 781, 96
- Marinoni, C., & Buzzi, A. 2010, Nature, 468, 539
- Matsubara T., & Suto, Y. 1996, ApJ, 470, L1
- McCavanna, T., Micic, M., Lewis, G. F., et al. 2012, MNRAS, 424, 361
- Morandi, A., & Sun, M. arXiv:1601.03741
- Outram, P.J., Shanks, T., Boyle, B.J., Croom, S.M., Hoyle, F., Loaring, N.S., Miller, L., & Smith, R.J. 2004, MNRAS, 348, 745
- Parejko J.K., et al., 2013, MNRAS, 429, 98
- Parihar, P., Vogeley, M.S., & Gott, J.R., et al. 2014, ApJ, 796, 86
- Park, C., Kim, J., & Gott, J.R. 2005, ApJ, 633, 1
- Park, C., & Kim, Y.-R. 2010, ApJL, 715, L185
- Park, C., Choi, Y.-Y., Kim, J., Gott, J.R., Kim, S.S., & Kim, K.-S. 2012, ApJ, 759, 7
- Park, C., Song, H., Einasto, M., Lietzen, H., & Heinamaki, P. 2015, JKAS, 48, 75
- Peebles, P.J.E., & Ratra, B. 2003, Reviews of Modern Physics, 75, 559
- Percival, W.J., Ross, A.J., & Sánchez, A.G., et al. 2014, MNRAS, 439, 2531
- Perlmutter, S., Aldering, G., & Goldhaber, G., et al. 1999, ApJ, 517, 565
- Press, W.H., & Schechter, P.L. 1974, ApJ, 187, 425
- Reid, B., Samushia, L., & White, M., et al. 2012, MNRAS, 426, 2719
- Reid, B., Ho, S., & Padmanabhan, N., et al. 2016, MNRAS, 455, 1553
- Riess, A.G., Filippenko, A.V., & Challis, P., et al. 1998, AJ, 116, 1009
- Riess, A.G., Macri, L., & Casertano, S., et al. 2011, ApJ, 730, 119
- Ross, A.J., Percival, W.J., & Sánchez, A.G. et al. 2012, MNRAS, 424, 564
- Ross, A.J., Samushia, L., & Howlett, C., et al. 2015, MNRAS, 449, 835
- Ryden, B.S. 1995, ApJ, 452, 25
- Sanchez, A. G., Scoccimarro, R., & Crocce, M., et al. arXiv:1607.03147
- Schlafly E.F., Finkbeiner D.P., Schlegel D.J., et al. 2010, ApJ, 725, 1175
- Schlafly E.F., & Finkbeiner D.P. 2011, ApJ, 737, 103
- Schlegel, D., Abdalla, F., & Abraham, T., et al. 2011, arXiv:1106.1706
- Smee, S.A., Gunn, J.E., & Uomoto, A., et al. 2013, AJ, 146, 32
- Song, Y.S., Sabiu, C.G., Okumura, T., Oh, M., & Linder, E.V. 2014, JCAP, 12, 005
- Speare, R., Gott, J.R., Kim, J., & Park, C. 2015, ApJ, 799, 176
- Viana, P.T.P., & Liddle, A.R. 1996, MNRAS, 281, 323
- Villalobos, Á., De Lucia, G., Weinmann, S.M., Borgani, S., & Murante, G. 2013, MNRAS, 433, L49
- Weinberg, S. 1989, Reviews of Modern Physics, 61, 1
- White M., et al. 2011, ApJ, 728, 126
- York, D.G., Adelman, J., & Anderson, J.E., et al. 2000, AJ, 120, 1579
- Zehavi, I., Zheng, Z., & Weinberg, D.H., et al. 2011, ApJ, 736, 59